Oxygen surface exchange and the significance of gas-phase mass transport

Ørjan Fossmark Lohne[a], Martin Søgaard[b] and Kjell Wiik[a]

[a]Department of Materials Science and Engineering, Norwegian University of Science and Technology, NO-7491 Trondheim, Norway
[b]Department of Energy Conversion and Storage, Technical University of Denmark, Frederiksborgvej 399, DK-4000 Roskilde

Abstract

In this work, the validity of electrical conductivity relaxation (ECR) as a method for the assessment of chemical surface exchange, k_{chem}, and bulk diffusion, D_{chem}, coefficients is investigated with respect to mass transport limitations in the gas phase. A model encompassing both the oxygen surface exchange, mass transport in the bulk sample and the gas phase was set up and solved under different conditions using finite element software. It is found that the transport of oxygen in the gas phase is insufficient at low oxygen partial pressures, causing a concentration boundary layer at the sample surface to develop. This significantly decreases the driving force for oxygen exchange. The effect of mass transport limitations on the computed apparent transport coefficients is shown to be pronounced and surface exchange coefficients are shown to deviate as much as one order of magnitude from the set values. When mass transport limitations are pronounced, a discrepancy between oxidation and reduction values of the apparent k_{chem} and D_{chem} is evident and modelled apparent activation energies for k_{chem} are shown to decrease significantly. The validity of the apparent transport coefficients can be improved by changing the experimental parameters, however the surface exchange coefficient is extremely sensitive to insufficient transport of oxygen in the gas phase and improvements are in general marginal. A criteria for the validity of D_{chem} is introduced while no such measure could be introduced for k_{chem}. The effect of experimental parameters and material properties on mass transport limitations are presented and general recommendations concerning the assessment of k_{chem} and D_{chem} are given.

1 Introduction

Development of new mixed ionic and electronic conducting materials (MIEC) have been of great interest for several years due to their potential use as oxygen gas separation membranes and SOFC fuel cells [1]. A key property of such materials is fast ionic and electronic conduction. In most cases, the electronic conductivity is much greater than the ionic conductivity and the performance of a material is then mainly determined by the oxygen transport properties [1, 2]. The characterization of oxygen transport kinetics is thus an essential part of research related to mixed ionic and electronic conducting (MIEC) materials and reliable characterization methods are a prerequisite. To be able to understand the transport properties of the materials, fundamental transport coefficients need to be obtained. Electrical conductivity relaxation (ECR) is a technique often used to obtain chemical surface exchange and bulk diffusion coefficients, k_{chem} and D_{chem}, respectively. The ECR method utilizes a dependency between the electronic conductivity and the oxygen non-stoichiometry of a MIEC material. By performing a step change in oxygen partial pressure, which will lead to a change in the oxygen non-stoichiometry, and monitoring the electronic conductivity response, the change in non-stoichiometry over time and thus the oxygen transport kinetics can be deduced. The validity of this technique, especially for materials exhibiting high oxygen exchange rates and/or at low partial pressures of oxygen, has however been questioned [3, 4]. In this study we will investigate the validity of ECR in terms of transport coefficient assessment both from an experimental and a theoretical modelling approach.

1.1 Motivation and initial results

Surface exchange and bulk diffusion coefficients obtained from ECR measurements have been shown to exhibit a discrepancy between steps performed from high to low (reduction) and low to high (oxidation) oxygen partial pressures in a number of reports [3, 4, 5, 6, 7]. The apparent difference in oxidation and reduction values is in general more pronounced at decreasing p_{O_2}. This is difficult to explain in terms of physical material properties, especially for bulk diffusion since the bulk diffusion coefficient should be independent of the direction of oxygen flux. A set of ECR measurements were initially carried out for this study on dense sintered $La_{0.2}Sr_{0.8}Fe_{0.8}Ta_{0.2}O_{3-\delta}$ (LSFTa) samples with dimensions $1 \times 3 \times 20$ mm in a reactor with a radius of 1 cm and a flow of 500 mL min^{-1}. The obtained D_{chem} and k_{chem} are shown in Fig. 1 where differences between oxidation and reduction values are clearly observed for both the surface exchange and bulk diffusion coefficient at low oxygen partial pressures. Oxygen transport during oxidation steps was controlled by surface exchange at low partial pressures of oxygen, thus, fitting of D_{chem} did not converge and bulk diffusion coefficients were not obtained at low p_{O_2}. The surface exchange coefficient decreases with decreasing p_{O_2} for both reduction and oxidation steps, while for the bulk diffusion coefficient, the oxidation values are increasing and the reduction values are decreasing with decreasing p_{O_2}. Both k_{chem} and D_{chem} show a more pronounced splitting between oxidation and reduction values at lower p_{O_2}.

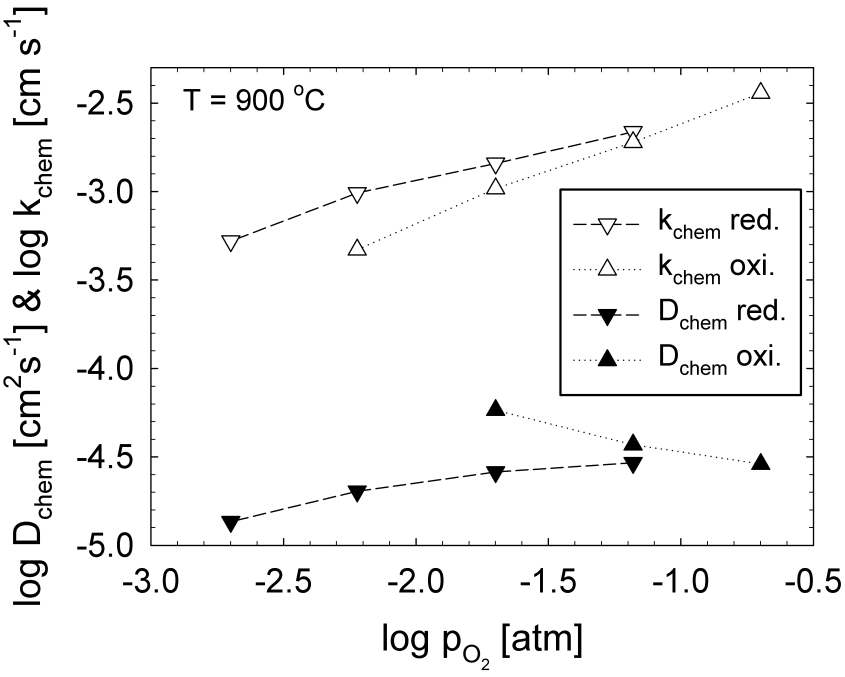

Fig. 1. Calculated k_{chem} and D_{chem} for LSFTa by electrical conductivity relaxation measurements. Lines are guide to the eye.

A vital prerequisite for using ECR as a method for assessing k_{chem} and D_{chem} is that the step change in oxygen partial pressure is close to discrete [8], i.e. the time required to establish the new p_{O_2} at the sample surface is negligibly small compared to the time required to bring the sample to the new equilibrium. In order to fulfil this requirement, the mass transport in the gas phase must be sufficiently effective to maintain the desired p_{O_2} at the sample surface after a step change in oxygen partial pressure, i.e. the p_{O_2} at the sample surface is independent on the rate of oxygen exchange. Insufficient mass transport at the sample surface will yield a concentration boundary layer with an oxygen concentration being higher than that of the bulk gas phase for reduction and lower than the bulk gas phase for oxidation. This will result in a gradual change in oxygen partial pressure and a reduction in driving force for oxygen exchange. The surface exchange and bulk diffusion coefficients deduced from such conditions will thus be apparent values, determined by the mass transport in the gas phase. Mass transport limitations in the gas phase combined with oxygen exchange of MIECs have been described in the literature before. Ben Mansour et al. [9] and Gozálvez-Zafrilla et al. [10] showed, through numerical modelling, that the steady-state flux measurements of a membrane setup were significantly influenced by mass transport in the gas phase. Also, for porous electrodes of MIECs in solid oxide fuel cells, gas transport limitations are well described [11]. In contrast, mass transport in the gas-phase are usually assumed to be fast and negligible as a rate determining mechanism for ECR measurements. However, the discrepancy between oxidation and reduction values of the surface exchange and bulk diffusion coefficients can not be explained by material properties and might be a result of mass transport limitations. In order to investigate whether mass transport in the gas phase could

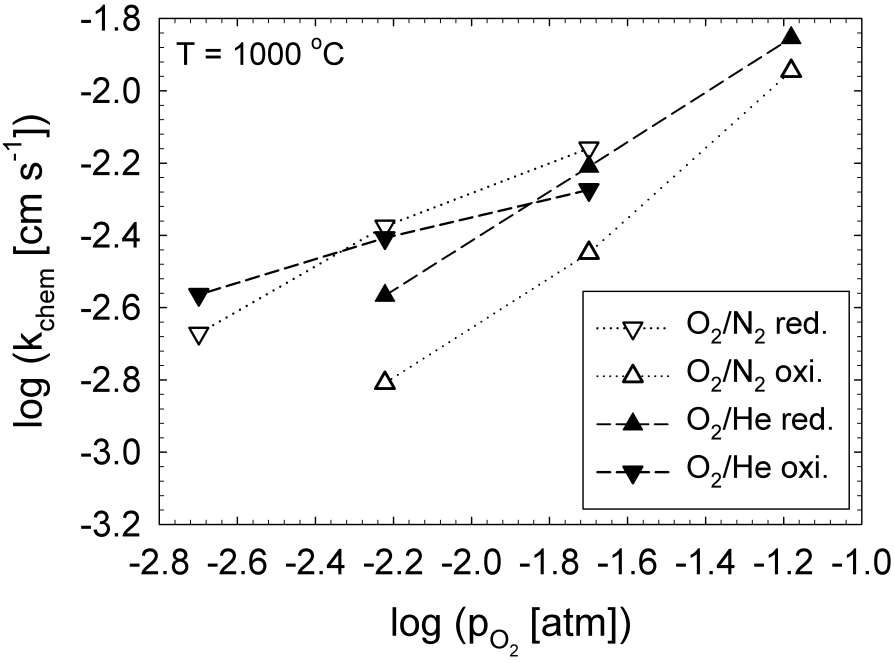

Fig. 2. Fitted values of k_{chem} for LSFTa by electrical conductivity relaxation measurements at 1000 °C using helium or nitrogen as carrier gas. Lines are guide to the eye.

have an effect on the apparent splitting between reduction and oxidation values, initial measurements were conducted comparing nitrogen and helium as a carrier gas. Helium is a gas with a low atomic mass compared to nitrogen and will thus improve the gas diffusion of oxygen by an increase in the binary gas diffusion coefficient [12]. The obtained surface exchange coefficients are shown in Fig. 2. It is evident that the discrepancy between k_{chem} obtained from oxidation and reduction runs is smaller for the measurements performed using helium as the carrier gas. This suggests that an effect of mass transport limitations might be present and that the discrepancy between oxidation and reduction values might be an effect of this. To further investigate the role of mass transport limitations in the gas phase in ECR measurements and its dependency on experimental parameters, a numerical modelling approach imitating a real measurement will be presented in this study.

2 Physical problem

This study focuses on electrical conductivity relaxation as a method for measuring oxygen surface exchange and bulk diffusion kinetics of oxides. For a perovskite, with the general formula $ABO_{3-\delta}$, the oxygen non-stoichiometry, δ, is dependent on the temperature and partial pressure of oxygen. The incorporation of oxygen into the lattice can be described by the red-ox reaction:

$$\tfrac{1}{2}\,\mathrm{O_2(g)} + \mathrm{V_O^{\bullet\bullet}} + 2\,\mathrm{e'} \rightleftharpoons O_O^x \tag{1}$$

written in terms of Kröger-Vink notation [13]. By a decrease in p_{O_2} Eq. (1) will shift to the left and the oxygen non-stoichiometry, δ, will increase and vice versa for an increase in p_{O_2}. The mass change of a material as a function of time after a discrete step in oxygen partial pressure can be measured. By fitting the obtained response to Fick's laws of diffusion combined with the appropriate boundary conditions, the surface exchange coefficient, k_{chem}, and bulk diffusion coefficient, D_{chem}, can be obtained. If the electrical conductivity of a material has a linear dependence with respect to the non-stoichiometry, one can use the conductivity as a measure of the change in oxygen non-stoichiometry. This method is referred to as electrical conductivity relaxation (ECR) [14].

When a step change in oxygen partial pressure is performed, oxygen is exchanged with the sample through a number of overall processes as given below:

1. Diffusive and convective transport of molecular oxygen gas from the gas stream to the sample surface.
2. Surface exchange: Adsorption of molecular oxygen onto the sample surface followed by a number of possible elementary reactions and finally incorporation into the lattice.
3. Diffusive transport of oxygen ions through the bulk of the sample.

In the typical equations used for fitting a transient in the electrical conductivity, it is assumed that the change in the surrounding oxygen partial pressure is infinitely fast. Thus, the chemical potential, or partial pressure, of oxygen should be constant throughout the bulk gas phase. A schematic of the oxygen chemical potential during an ECR step is shown in Fig. 3. The blue line schematically represents the chemical potential of oxygen across the reactor and sample with the changes in chemical potential attributed to each of the numbered processes above. In Fig. 3 (a), the mass transport in the gas phase is sufficiently fast, while in Fig. 3 (b), mass transport limitations are significant, yielding a chemical potential gradient in the gas phase. The aim of this study is to investigate how gas phase mass transport affects the determination of fundamental transport coefficients such as k_{chem} and D_{chem}.

2.1 Oxygen surface exchange and bulk diffusion

According to Eq. (1), a change in the partial pressure of oxygen will result in a net flux of oxygen in or out of the sample. The flux of oxygen in the sample can be described in terms of the chemical bulk diffusion coefficient, D_{chem}, and is obtained by solving Fick's second law of diffusion:

$$\frac{\partial C_O(x,t)}{\partial t} = D_{chem}\frac{\partial^2 C_O(x,t)}{\partial x^2} \tag{2}$$

where C_O is the concentration of oxygen ions in the sample. The boundary condition at the sample surface is given by the definition of the surface exchange coefficient:

$$J_{O,surf} = k_{chem}\Delta C_O \tag{3}$$

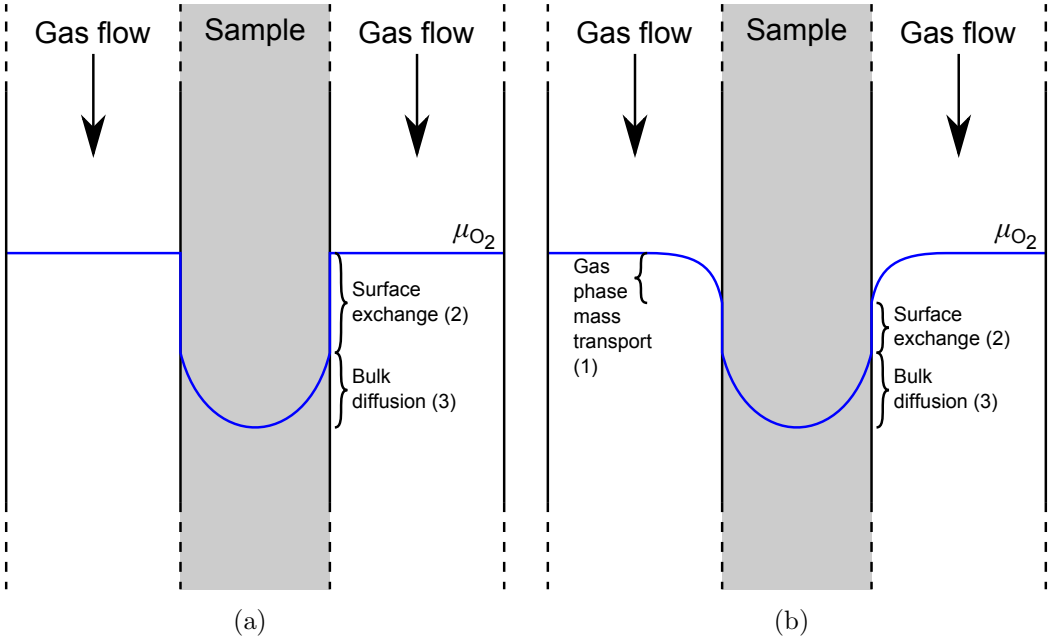

Fig. 3. A qualitative schematic of the oxygen chemical potential and different oxygen transport processes during a ECR measurement. (a) An ideal case where mass transport in the gas phase is sufficiently effective and (b) a case with insufficient gas phase mass transport yielding a concentration boundary layer at the sample surface.

where $J_{O,surf}$ is the flux of monoatomic oxygen across the surface, k_{chem} is the chemical surface exchange coefficient and $\Delta C_O = (C_{O,surf} - C_{O,eq})$ where $C_{O,surf}$ is the actual concentration of oxygen in the surface and $C_{O,eq}$ is the final equilibrium concentration of oxygen at the p_{O_2} given. The solution of Eqs. (2) and (3) have been thoroughly described elsewhere [8, 15] and is given in Appendix A.

3 Model formulation

This study has been carried out by performing computational modelling using finite element analysis. The commercially available COMSOL Multiphysics® 4.2 was used as software with the built-in "CFD" (Computational Fluid Dynamics), "Chemical reaction engineering", and "AC/DC" software modules where each module contains a predefined selection of physical equations governing different properties. A schematic of the geometric setup of the model is shown in Fig. 4. A 2-dimensional axi-symmetric model has been built to minimize the computational efforts. Two different coupled domains were used; a gas phase reactor and a solid sample. The top horizontal boundary of the reactor serves as a laminar flow inlet while the bottom horizontal boundary is the flow outlet. The conductivity of the material was measured in a similar manner as for a real ECR measurement [14]. Hence, the top and bottom horizontal surfaces of the sample have been defined as current electrodes, passing a constant current through the sample while the electric potential over two

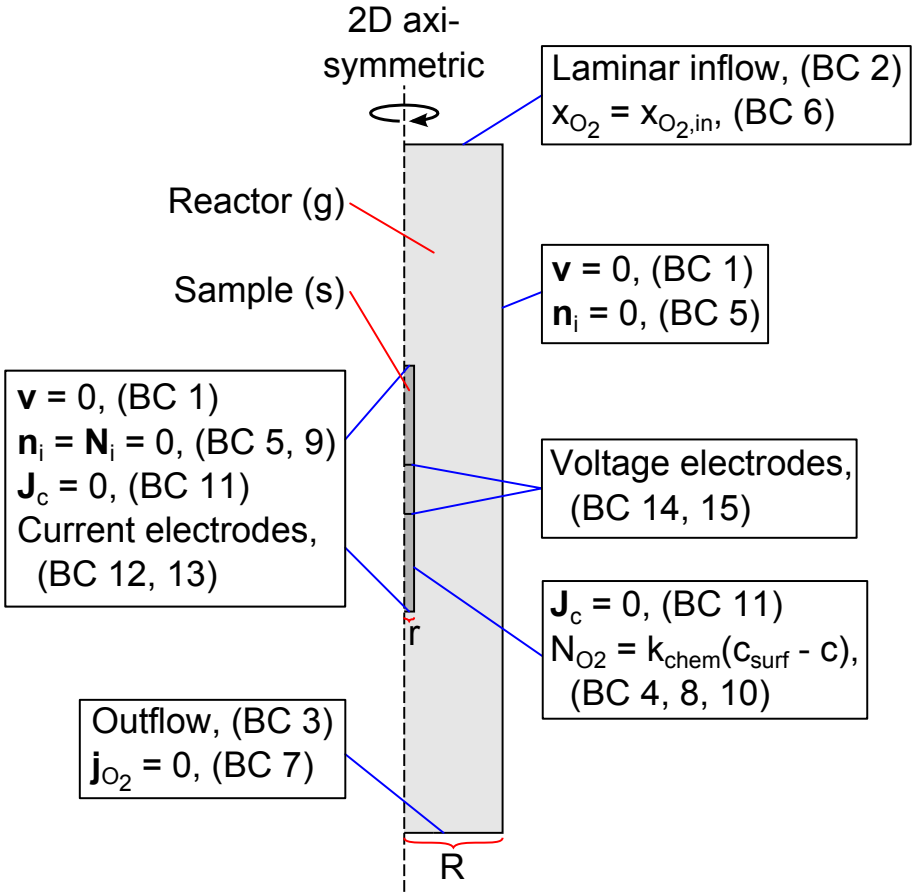

Fig. 4. A schematic of the developed model with defined boundary conditions (BC), blue lines, and geometric entities, red lines.

horizontal, 1-dimensional, lines (voltage electrodes) across the sample is monitored. The conductivity is then calculated according to:

$$\sigma = \frac{l}{A} \cdot \frac{I}{V} \tag{4}$$

where l is the distance between the voltage electrodes, A is the cross sectional area of the sample, I is the current passed through the sample and V is the electric potential over the voltage electrodes. The calculated conductivity transient is then used to calculate k_{chem} and D_{chem} as described in section 2.1. The dimensions of the setup and material properties were chosen to mimic a real ECR setup and are presented in section 3.4.

3.1 Governing equations

To model the fluid dynamics (gas flow) in the reactor, the "Laminar flow" physic in the "CFD" module was chosen. The general governing equations used were the conservation of momentum (Navier-Stokes equation, Eq. (5)) and conservation of

mass (continuity equation, Eq. (6)), viz:

$$\frac{\partial \rho \mathbf{v}}{\partial t} + \rho(\mathbf{v} \cdot \nabla)\mathbf{v} = -\nabla p \tag{5}$$

$$\frac{\partial \rho}{\partial t} + \nabla \cdot (\rho \mathbf{v}) = 0 \tag{6}$$

where $\mathbf{v}$ [m s^{-1}] is the velocity, ρ [kg m^{-3}] is the density of the gas and p [Pa] is the total pressure of the gas. Vector quantities are denoted with bold characters. For simplicity Eq. (5) is written assuming no viscous stresses as the effect of viscous stresses are assumed negligible for the conditions applied in this study, although the software do include this in the computation. The density, ρ, and dynamic viscosity, μ [Pa s^{-1}], of the gas were assumed to be those of the carrier gas, either nitrogen or helium, and were given as a function of temperature and pressure by the built-in material database in COMSOL. Eqs. (5) and (6) are solved assuming laminar flow only. The dimensionless Reynolds number, Re, is usually introduced as a measure of the flow characteristics in fluid flow and expresses the ratio between inertial and viscous forces on the fluid. The Reynolds number for fluid flow in a pipe can be calculated from [16]:

$$\mathrm{Re} = \frac{\rho v_{av} D}{\mu} \tag{7}$$

where v_{av} [m s^{-1}] is the average velocity of the fluid and D [m] is the diameter of the pipe. For an circular annulus, such as between the sample and reactor wall, D can be expressed as $D = 2(R - r)$ where R is the diameter of the outer tube and r is the diameter of the inner tube. The transition from laminar to turbulent flow is considered to take place at Reynolds numbers Re > 2100 for flow in a pipe and Re > 2000 for flow in an annulus [16]. For smaller Reynolds numbers the flow is considered to be stable and laminar. For the dimensions considered in the following, Reynolds numbers below 100 are obtained in all cases, thus the flow is assumed fully laminar.

The mass transport in the gas phase was solved using the "Transport of concentrated species" physic in the "Chemical reaction engineering" module. A computational inexpensive mixture-averaged diffusion model, which assumes a concentration independent diffusion coefficient, was used. This assumption was tested by performing a model run using the common, but computationally more demanding, Maxwell-Stephan diffusion model for comparison. No significant differences were observed, therefore this assumption is considered viable. The governing equation for the mass transport in the gas phase is the mass balance equation:

$$\frac{\partial \rho \omega_{O_2}}{\partial t} + \nabla \cdot (\rho \mathbf{v} \omega_{O_2}) + \nabla \cdot \mathbf{j}_{O_2} = 0 \tag{8}$$

where ω_{O_2} is the mass fraction of oxygen in the gas, $\mathbf{v}$ is the velocity field solved by the "Laminar flow" physic and $\mathbf{j}_{O_2}$ is the diffusive mass flux of oxygen in the gas, viz:

$$\mathbf{j}_{O_2} = -\rho D^m_{O_2} (\nabla \omega_{O_2} + \omega_{O_2} \frac{\nabla M_n}{M_n}) \tag{9}$$

where M_n is the mixture-averaged molar mass:

$$M_n = \left(\sum_i \frac{\omega_i}{M_i} \right)^{-1} \tag{10}$$

and $D_{O_2}^m$ is the mixture averaged oxygen diffusion coefficient, given by:

$$D_{O_2}^m = \frac{1 - \omega_{O_2}}{\frac{x_{N_2}}{D_{O_2N_2}}} \tag{11}$$

where $D_{O_2N_2}$ is the binary diffusion coefficient in a O_2/N_2 gas mixture. $D_{O_2N_2}$ was estimated by [12]:

$$D_{O_2N_2} = \frac{0.00266T^{3/2}}{PM_{O_2N_2}^{1/2}\sigma_{O_2N_2}^2\Omega_D} \tag{12}$$

where T is the temperature [K], P is the pressure [bar], $M_{O_2N_2} = 2[(1/M_{O_2}) + (1/M_{N_2})]^{-1}$ where M_{O_2} and M_{N_2} are the molecular weights of O_2 and N_2 [g mol^{-1}], $\sigma_{O_2N_2}$ is the characteristic length of the intermolecular force law [Å] and Ω_D is the collision integral for diffusion. $\sigma_{O_2N_2}$ are given by:

$$\sigma_{O_2N_2} = \frac{\sigma_{O_2} + \sigma_{N_2}}{2} \tag{13}$$

where $\sigma_{O_2} = 3.467$ Å, $\sigma_{N_2} = 3.798$ Å and $\sigma_{He} = 2.551$ Å are tabulated values [12]. For calculation of Ω_D the reader is referred to Eq. (11-3.6) in [12]. When modelling with helium as the carrier gas, all the N_2 subscripted properties given in the above calculations have been changed to those of helium.

For the transport of oxygen ions in the solid sample, the "Transport of diluted species" physic in the "Chemical reaction engineering module" was used. The concentration of oxygen at a given time and coordinate was modelled by solving the mass balance equation:

$$\frac{\partial C_O}{\partial t} + \nabla \cdot \mathbf{J}_{O,bulk} = \frac{\partial C_O}{\partial t} + \nabla \cdot (-D_{chem} \nabla C_O) = 0 \tag{14}$$

where $\mathbf{J}_{O,bulk}$ is the diffusive molar flux of monoatomic oxygen in the bulk sample. Eq. (14) is written assuming only diffusive transport and no reactions.

For the electric currents in the sample domain, the "Electric Currents" physic in the "AC/DC" module was used. The electric current in the sample was modelled by solving the charge conservation equation:

$$\nabla \cdot \mathbf{J}_c = \nabla \cdot (\sigma \mathbf{E}) = 0 \tag{15}$$

where $\mathbf{J}_c$ [A cm^{-2}] is the current density, σ [S cm^{-1}] is the electrical conductivity and $\mathbf{E}$ [V m^{-1}] is the electric field defined from $\mathbf{E} = -\nabla V$, where V [V] is the electric potential.

3.2 Boundary conditions

The boundary conditions used in the model are schematically presented in Fig. 4.

For the "Laminar flow" physic in the reactor domain, four boundary conditions were employed:

1. Non-slip conditions, $\mathbf{v} = 0$, were set to the reactor wall and the top and bottom surfaces of the sample
2. The inlet at the top end of the reactor was set to laminar inflow with a defined volumetric flow rate and an entrance length of 0.1 m
3. The outlet at the bottom end of the reactor was set to no overpressure, $p_0 = 0$ Pa, and assuming no viscous stress
4. The inlet at the sample side surface was set to a "Pointwise mass flux":
   $n_{O_2} = -k_{chem} \cdot (C_{O,surf} - C_O) \cdot (M_{O_2}/2)$ [kg m^{-2} s^{-1}]
   where $C_{O,surf}$ is the equilibrium concentration of oxygen ions for the actual p_{O_2} at the surface and C_O is the actual oxygen ion concentration in the sample surface solved by the "Transport of diluted species" physic.

The last boundary condition is important when only one species in a multicomponent system is exchanged across a boundary in a domain. This becomes evident when considering the mass average velocity, $\mathbf{v}$, which is given by the sum of all mass fluxes, $\mathbf{n}_i$, [16]. For a general binary system with species A and B this can be written as:

$$\rho\mathbf{v} = \mathbf{n}_A + \mathbf{n}_B \tag{16}$$

If only species A is exchanged across a boundary, $\mathbf{n}_A$ is non-zero and $\mathbf{n}_B = 0$ at the boundary. This leads to:

$$\mathbf{v} = \mathbf{n}_A/\rho \tag{17}$$

Hence, $\mathbf{v}$ is non-zero and therefore a non-slip boundary condition can not be used.

For the "Transport of concentrated species" physic in the reactor domain, four boundary conditions were employed:

5. No-flux conditions, $\mathbf{n}_i = 0$, were set for all species at the reactor wall and the top and bottom surfaces of the sample
6. An inflow condition at the top end of the reactor was set to a mole fraction of O_2 as a piecewise step function, changing from $x_{in,O_2} = x_{0,O_2}$ to $x_{in,O_2} = x_{O_2} \neq x_{0,O_2}$ after a given time $t > 0$
7. An outflow condition, $\mathbf{j}_{O_2} = 0$, was set at the bottom end of the reactor
8. A flux condition was set to the sample side surface as an inward mass flux of oxygen, $n_{O_2} = -k_{chem} \cdot (C_{O,surf} - C_O) \cdot (M_{O_2}/2)$ [kg m^{-2} s^{-1}]

The piecewise step function of boundary condition 6 was set to "no smoothing" to make a discrete step for the partial pressure change.

For the "Transport of diluted species" physic in the sample domain, two boundary conditions were employed:

9. No flux conditions, $\mathbf{N}_i = 0$, were set at the top and bottom (horizontal) surfaces of the sample
10. A flux condition was set to the sample side surface as a general inward mole flux, $N_O = k_{chem} \cdot (C_{O,surf} - C_O)$ [mol m^{-2} s^{-1}], (allow the sample to exchange oxygen)

The surface exchange reaction, Eq. (1), is a total reaction and may consist of a number of elementary reactions such as adsorption, dissociation/association of the oxygen molecule, charge transfer and incorporation/excorporation of oxygen in/out of the vacancies. The different elementary reactions are not resolved in this model and hence boundary conditions 4, 8 and 10 have been set to treat all elementary reactions as one global reaction with the general kinetic parameter k_{chem}.

For the "Electric currents" physic in the sample domain, five boundary conditions were employed:

11. Electric insulation, $\mathbf{J}_c = 0$, was set to the vertical sample surface
12. An electric potential node was set to the top horizontal sample surface with a voltage $V = 0$
13. A circuit terminal was applied to the bottom horizontal sample surface
14. Each of the two voltage electrodes were chosen as a current terminal. The terminal current was set to $I_{term} = 0$ in order not to influence the current distribution in the sample.
15. See 14

The "Electric circuits" physic in the "AC/DC" module was used to connect the electric potential node and the circuit terminal (boundary condition 12 and 13) with a current source. The electric potential node serves as a ground node and negative electrode and the circuit terminal serves as the positive electrode while a current source, I_{src} [A], was applied over the circuit.

3.3 Meshing

The mesh type used is a non-uniform, triangular mesh. Three different mesh element sizes have been refined, one for each of the domains (solid sample and gas phase reactor) and one for the boundary at the sample surface. Built-in predefined element sizes were chosen to build the mesh. The element size for the reactor domain were set to "Coarse" and chosen to be calibrated for fluid dynamics. The element size for the sample domain and sample surface boundary were set to "Normal" and "Extra fine", respectively, and were chosen to be calibrated for general physics. The number of elements for the complete mesh for different reactor radii is given in Table 1 and a detailed drawing of the mesh for a reactor radius $R = 1$ cm

Table 1. Number of mesh elements in different geometric entities.

Reactor radius, R [cm]	# of elements in reactor domain	sample domain	total
1	7833	2132	9965
0.5	14885	4967	19852
0.25	27929	10721	38650

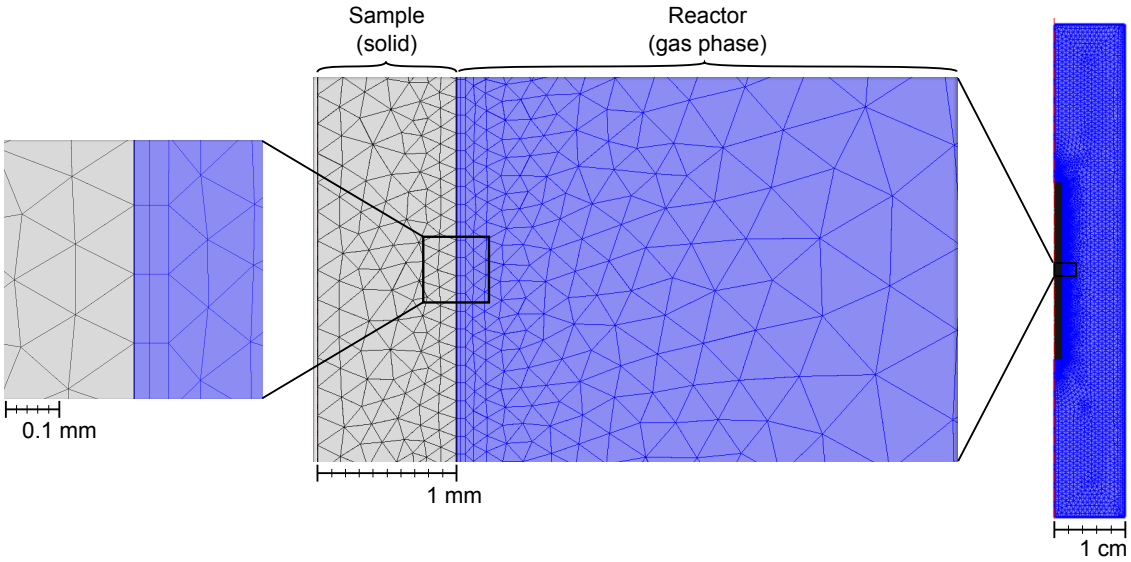

Fig. 5. Detail of the meshes used in the different domains for a reactor radius $R = 1$ cm.

is shown in Fig. 5. In order to ensure that the solution is independent of the mesh size, a series of model runs were performed with different mesh sizes. The modelling was performed with a p_{O_2} step from $p_{O_2,start} = 2 \cdot 10^{-2}$ atm to $p_{O_2,final} = 6.6 \cdot 10^{-3}$, a reactor radius $R = 1$ cm and a sample radius $r = 1$ mm. The number of meshing elements were changed by adjusting the mesh size setting for the sample surface boundary. Chemical surface exchange and bulk diffusion coefficients were calculated from the modelled conductivity transient, as described in section 3. The modelled coefficients as a function of the number of meshing elements are shown in Fig. 6. The calculated values of both k_{chem} and D_{chem} converge at ≈10000 number of elements. With an increase in number of elements from 9965 to 18693, the improvement in the calculated transport coefficients is only marginal and due to the increasing computational effort with larger number of elements, the settings with 9965 elements were used. When using the predefined mesh sizes as described above, the software adjusts the number of elements to the geometrical size of the model domains. Consequently, for reactor radii 0.5 cm and 0.25 cm, the number of elements is significantly increased (cf. Table 1). Hence, the model runs using the smaller reactor radii are assumed to be even more accurate.

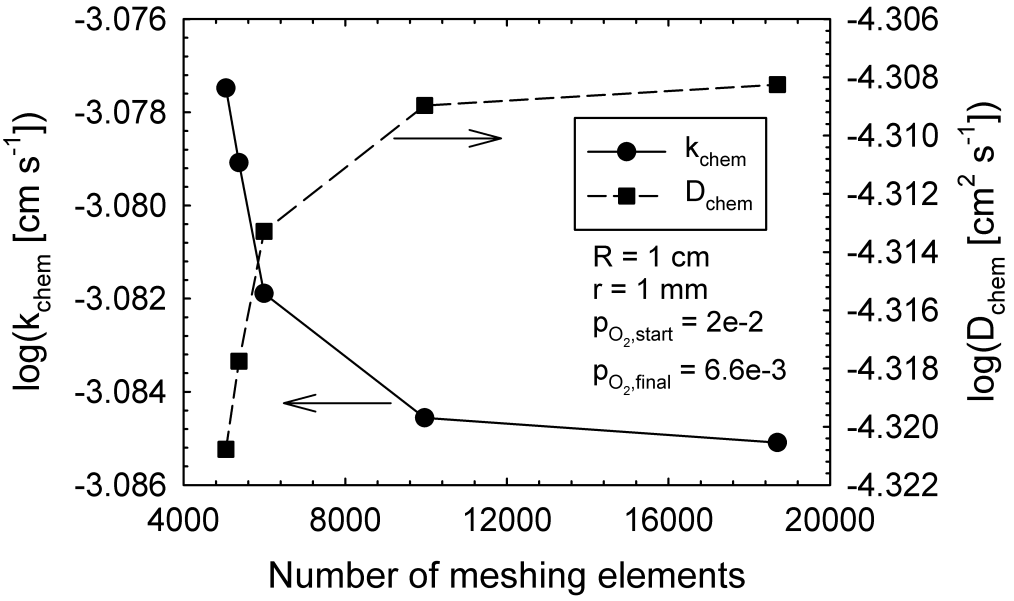

Fig. 6. Convergence of k_{chem} and D_{chem} with number of meshing elements.

3.4 Model input

The length of the reactor and the sample are set to 7 cm and 2.5 cm, respectively. The centre of the sample is vertically positioned at half the reactor length. The voltage electrodes are positioned symmetrical around the half sample length with a distance between the electrodes of 5 mm. The temperature is kept constant throughout the model entity and any potential effect of joule heating due to the current passed through the sample is disregarded.

The presented data obtained from theoretical modelling in this report have been performed using material properties based on reported data for $Ba_{0.5}Sr_{0.5}Co_{0.8}Fe_{0.2}O_{3-\delta}$ (BSCF) [5, 17] and are summarized in Table 2. The oxygen non-stoichiometry, $3-\delta$, is set to be linear with $\log p_{O_2}$ to ensure that the total uptake or release of oxygen, $\Delta\delta$, with a constant $\log p_{O_2}$ step size is independent on the partial pressure of oxygen. The total change in oxygen stoichiometry, $\Delta\delta$, with a step-size of half an order of magnitude in the oxygen partial pressure region $1 \cdot 10^{-3} \leq p_{O_2} \leq 0.209$ atm for a selection of perovskite materials are shown in Table 3. The change in non-stoichiometry for the model material is comparable with some commonly studied compositions in the (La,Sr)(Fe,Co)$O_{3-\delta}$ system. The conductivity is set to be linear with the oxygen stoichiometry to ensure that the condition for applying conductivity as a measure of the mass change is fulfilled [14]. For the materials and the oxygen partial pressure range modelled here, the ionic conductivity is negligible compared to the electronic. Thus the total conductivity is equal to the electronic conductivity.

Table 2. COMSOL model input parameters

Property		Value
Global		
T	[°C]	900
Flow	[ml min^{-1}]	$500 \cdot (T$ [K]/293.15 K)
$D_{O_2N_2}$	[cm^2 s^{-1}]	2.1
D_{O_2He}	[cm^2 s^{-1}]	4.5
I_{src}	[A]	0.5
Material specific		
ρ	[g cm^{-3}]	5.56
δ		$-2.9 \cdot 10^{-2} \cdot \log p_{O_2} + 4.8 \cdot 10^{-1}$
σ	[S cm^{-1}]	$300 \cdot (3 - \delta) - 600$
k_{chem}	[cm s^{-1}]	$8 \cdot 10^{-3}$
D_{chem}	[cm^2 s^{-1}]	$1.5 \cdot 10^{-4}$

Table 3. Total change in oxygen non-stoichiometry, $\Delta\delta$, at 900 °C with a step change in p_{O_2} of half an order of magnitude in the oxygen partial pressure region $1 \cdot 10^{-3} \leq p_{O_2} \leq 0.209$ atm for selected materials.

Material	$\Delta\delta$	Ref.
Model material	0.0145	-
$La_{0.2}Sr_{0.8}FeO_{3-\delta}$	0.013–0.023	[18]
$La_{0.6}Sr_{0.4}CoO_{3-\delta}$	≈ 0.019	[19]
$La_{0.6}Sr_{0.4}Co_{0.4}Fe_{0.6}O_{3-\delta}$	≈ 0.018	[20]

4 Results and discussion

4.1 The effect of gas-phase oxygen transport limitations

The normalized logarithmic oxygen partial pressure modelled at the sample surface is shown in Fig. 7 (a) as a function of time from oxidation and reduction steps with final partial pressure of oxygen $p_{O_2,final} = 6.6 \cdot 10^{-3}$ atm and a step-size of half an order of magnitude. The oxygen partial pressure is here normalized as $\log p_{O_2,start} = 1$ and $\log p_{O_2,final} = 0$ to better compare oxidation and reduction steps. Data from modelling an ideal case where the composition of the gas phase is independent of the oxygen flux over the sample surface is also included. This reflects a case where the binary gas diffusion constant $D_{O_2N_2}$ equals infinity and was performed by disabling the boundary conditions at the sample surface for the physics governing the gas phase. The conductivity is modelled as described in section 3 and normalized conductivities from the same relaxations as above are shown in Fig. 7 (b). The oxygen partial pressure at the sample surface drops abruptly at the

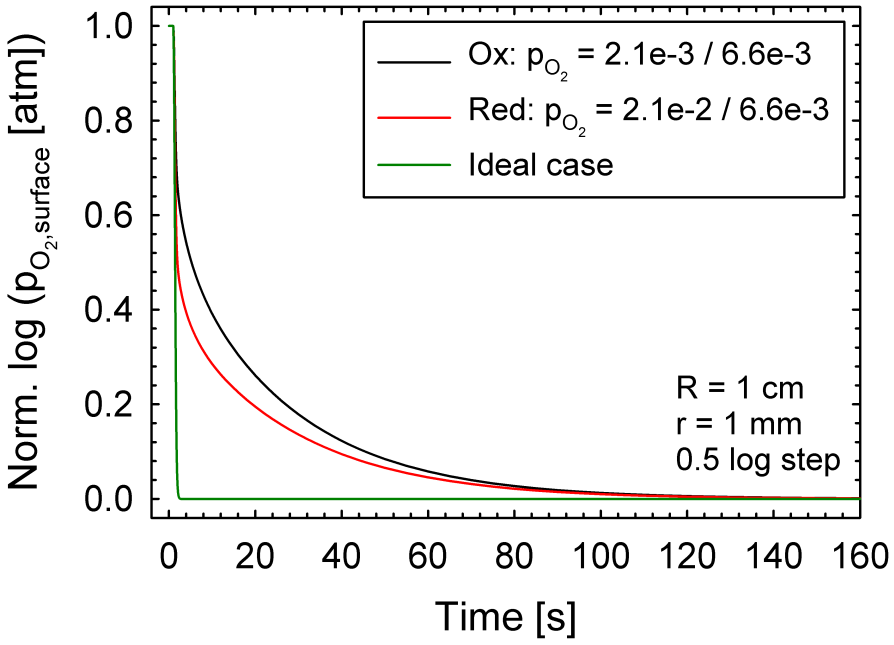

(a)

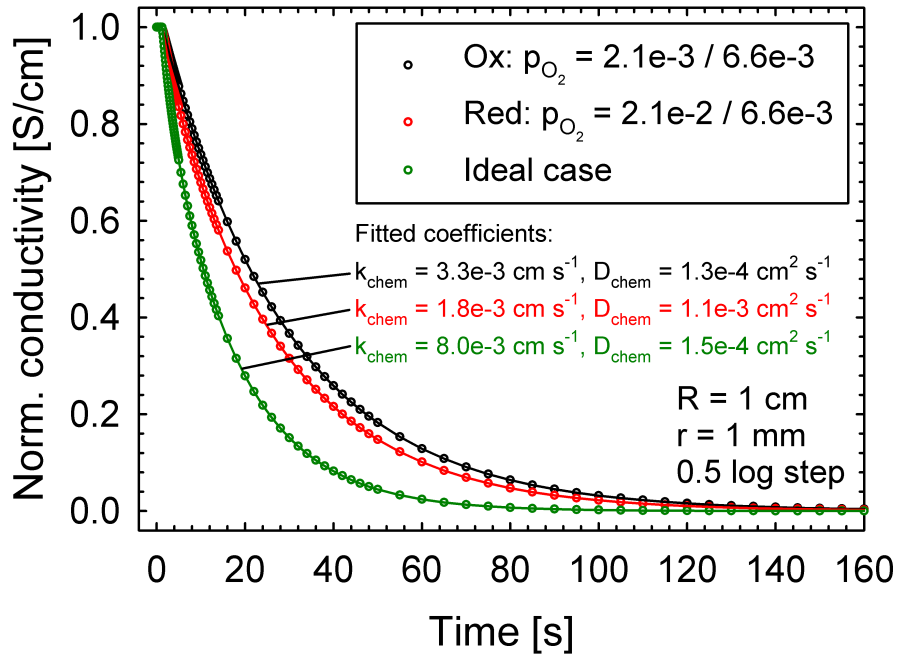

(b)

Fig. 7. (a) Normalized partial pressure of oxygen at the sample surface. (b) Normalized conductivity as a function of time from the developed model with solid lines representing the fit to the data as described in section 2.1. p_{O_2} step is $2.1 \cdot 10^{-2} - 6.6 \cdot 10^{-3}$ atm for reduction and $2.1 \cdot 10^{-3} - 6.6 \cdot 10^{-3}$ atm for oxidation.

start of the relaxation, but only to about half the value of the intended step. It takes approximately 150 s for the oxygen partial pressure at the sample surface to reach the same value as the partial pressure of the inlet gas, clearly showing insufficient mass transport in the gas phase. After 150 s the conductivity relaxation is also close to equilibrium, Fig. 7 (b). Hence, comparing the time scale of the conductivity relaxation and the partial pressure change at the sample surface, it is evident that the concentration boundary layer at the surface significantly affect the relaxation. The magnitude of the effect on the conductivity relaxation can clearly be seen in Fig. 7 (b) where the conductivity relaxations for the real cases deviate strongly from that of the ideal case. A difference between the oxidation and reduction runs can be seen for the real case which will be further discussed in section 4.2.

Chemical surface exchange and bulk diffusion coefficients were calculated from the modelled conductivity transient, as described in section 3. The obtained coefficients when modelling with (red plots) and without (green plots) the surface flux boundary condition enabled in the gas phase, respectively, are shown in Fig. 8. The solid lines represent the input values of the transport coefficients for the developed model, as given in Table 2. The data points represent the modelled coefficients from the conductivity data obtained from the model with upward triangles for oxidation and downward triangles for reduction. The model runs for the ideal case were used as part of the validation of the model. As seen, the modelled coefficients for the ideal case, green plots, do not deviate from the input coefficients. Hence

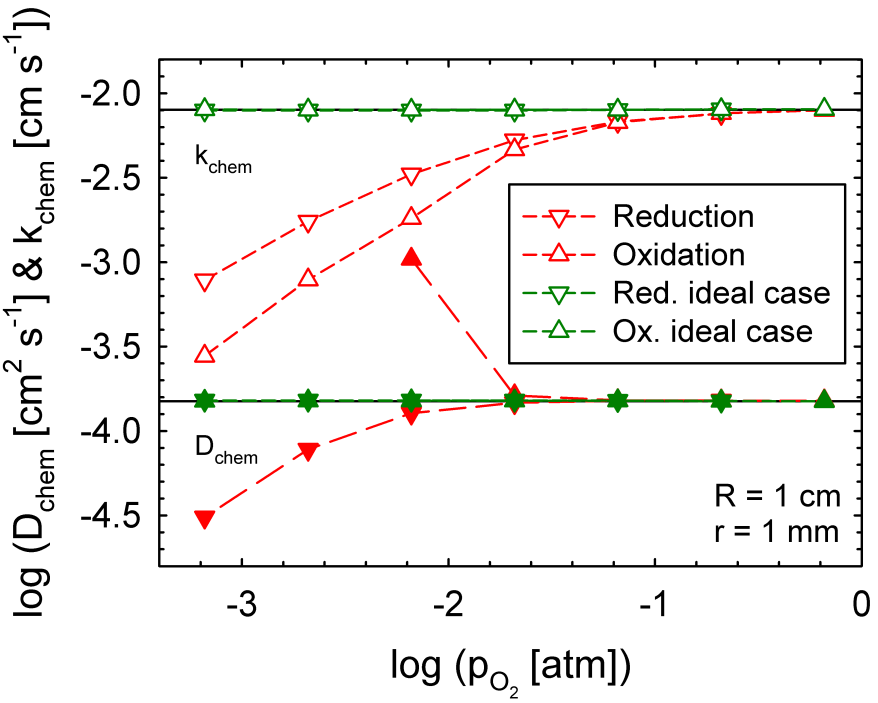

Fig. 8. Fitted k_{chem} and D_{chem} from modelled conductivity data. Solid lines represent the input coefficients to the model. R and r are reactor and sample radius, respectively, as defined in Fig. 4

the developed model and the ECR fitting procedure proves valid. There is a clear deviation between the input and the calculated coefficients for the real case. Hence the the coefficients at low p_{O_2} are apparent values, significantly influenced by mass transport limitations. Both the reduction and oxidation values of the apparent k_{chem} are decreasing with decreasing p_{O_2}. At sufficiently low oxygen partial pressure the reduction and oxidation values even split with the latter being the lowest. The apparent D_{chem} shows a splitting between oxidation and reduction values in the same region as the deviation in k_{chem} becomes pronounced. Regarding transport coefficients extracted from real ECR measurements (Fig. 1) the trends in D_{chem} are very similar to the modelled case (Fig. 8) and it is also likely that part of the k_{chem} dependency with p_{O_2} is an apparent dependency influenced by a deviation from true values. The reason for the deviation in the apparent transport coefficients is due to mass transport in the gas phase being a rate-determining process.

4.2 Effect of experimental parameters on gas-phase oxygen transport limitations

To reduce the concentration boundary layer, oxygen needs to be transported towards or away from the sample more effectively during a relaxation. The mass transport in the gas phase can be calculated from the solution of the mass balance equation, Eq. (8). The convection term in the mass balance is dependent on the gas velocity while the diffusion term, Eq. (9), is dependent on the binary diffusion coefficient and the gradient in mass fraction. Hence, mass transport by convection can be increased by increasing the velocity and mass transport by diffusion can be increased by increasing the binary diffusion coefficient and the gradient in mass fraction. The effect of a change in the above mentioned parameters will be presented later in this section.

A change in the total amount of oxygen exchanged during a relaxation might also affect the concentration boundary layer. This can be performed either by changing the partial pressure step size, which determines the magnitude of change in non-stoichiometry, $\Delta\delta$, or changing the sample size, which determines the extent of the oxygen reservoir in the sample. The results of model runs with different step sizes are shown in Fig. 9. At high oxygen partial pressures, the deviation of the chemical surface exchange coefficient, k_{chem}, is small and independent of the p_{O_2} step-size and true values are obtained at $p_{O_2} \geq 0.1$ atm. At lower oxygen partial pressures, the deviation is more pronounced and a splitting between coefficients obtained from reduction and oxidation steps, being more pronounced for larger step-sizes, is observed. However, decreasing the step size does not reduce the deviation of the surface exchange coefficients, but merely decreases the gap between oxidation and reduction values. According to Eq. (3), decreasing the step size, and consequently also ΔC_O, will decrease the flux of oxygen across the surface. However, the amount of exchanged oxygen needed to have the same relative effect on the p_{O_2} will be correspondingly smaller. Hence, the magnitude of mass transport limitations is independent of the oxygen partial pressure step size. The more pronounced splitting between oxidation and reduction values at larger step sizes is merely a result

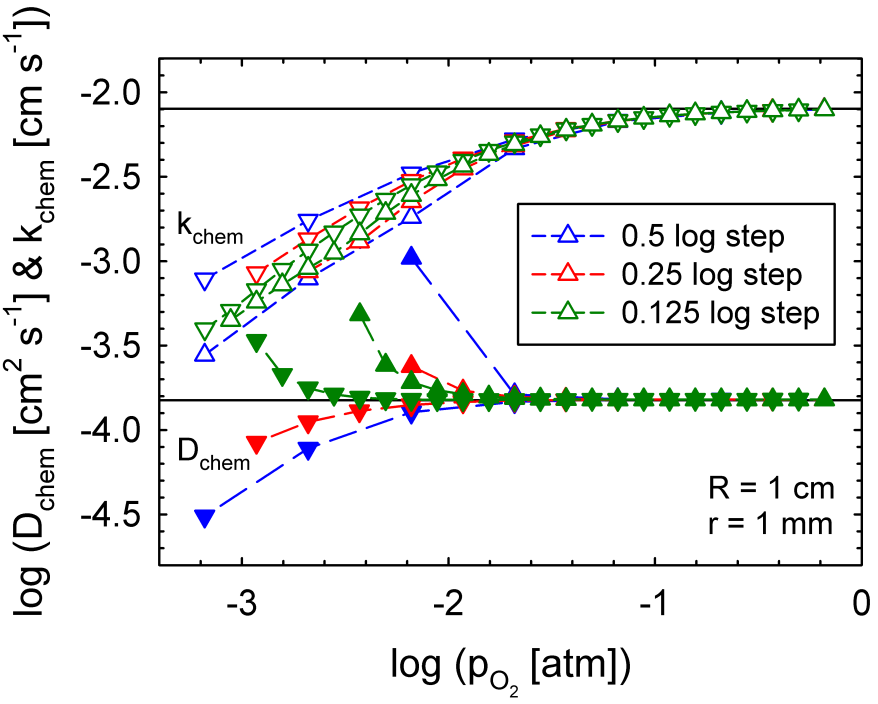

Fig. 9. Fitted k_{chem} (open symbols) and D_{chem} (closed symbols) from modelled conductivity data with different oxygen partial pressure step sizes. Oxidation values are given as upward triangle symbols while reduction values appear as downward triangle symbols.

of k_{chem} being plotted against final p_{O_2}. As mentioned in section 4.1, the $\log p_{O_2}$ step change in the initial part of the relaxation is smaller than the intended step when mass transport limitations are present. During the initial part of a step only a small amount of oxygen have been exchanged with the sample and the concentration gradient is large in the surface and small in the bulk. According to Eq. (2) and (3), this implies that the oxygen flux in the sample is mainly determined by the surface exchange coefficient. After some time, the gradient in the bulk becomes large and the oxygen flux in the sample is then mainly governed by bulk diffusion. Hence, calculations of the surface exchange coefficient is highly determined by the initial part of the conductivity relaxation. Accordingly, the calculation of k_{chem} from the conductivity relaxation when mass transport limitations are present will be determined at a p_{O_2} higher than the applied final oxygen partial pressure for reduction and vice versa for oxidation. In Fig. 7 (a) it was shown that at $p_{O_2,final} = 6.6 \cdot 10^{-3}$ atm the initial step size was around half the value of the intended step. It can be seen in Fig. 9 that the surface exchange coefficients at low p_{O_2} will approximately be equal for oxidation and reduction if the reduction values are shifted to higher p_{O_2} by approximately half a step size and vice versa for oxidation values. It is also not applicable to use the splitting of oxidation and reduction values as an accurate measure of validity for the apparent coefficients as the apparent splitting occurs at a p_{O_2} where the deviation is already pronounced.

In Fig. 9, a splitting between oxidation and reduction values is also observed for D_{chem}, being less pronounced when reducing the step size. Regarding the deviation in D_{chem} the calculated apparent coefficients possess no deviation from the true coefficients until the splitting between the oxidation and reduction values occur. Hence, we can introduce a measure of validity for D_{chem} stating that, as long as there is no pronounced splitting between coefficients obtained from oxidation and reduction runs, the calculated D_{chem} can be trusted as valid. However, the cut-off p_{O_2} for the D_{chem} is obviously an insufficient criteria for the validity of k_{chem} since the onset of deviation for the surface exchange coefficient is at higher oxygen partial pressures than that of the bulk diffusion coefficient. We can then conclude that the deviation of the apparent k_{chem} due to mass transport limitations in the gas phase is independent of the step size of the relaxation. Also, the onset p_{O_2} for an apparent splitting of D_{chem} oxidation and reduction values can be introduced as an accurate criteria for the validity of D_{chem} while no such measure can be introduced for k_{chem}.

To increase the transport of oxygen in the gas phase near the sample surface, convection or diffusion of oxygen needs to be enhanced. Convection can be enhanced by simply increasing the flow rate or decrease the reactor radius while keeping the volumetric flow rate constant, both measures will increase the average velocity of the gas and presumably sweep more efficiently over the sample surface. Turbulent flow will also be expected to increase the convective mass transport close to the surface. The cross sectional area of the reactor along the sample, $A_{CS} = A(R) - A(r)$, the average gas velocity and the Reynolds number over this cross-section for different reactor radii are given in Table 4. The Reynolds numbers are all small and considerably smaller than the transition to a turbulent regime at Re $\approx$ 2100 [16]. Thus the possible effect of turbulent flow will not be further addressed. Nevertheless, the average velocity of the gas is increased significantly by decreasing the reactor radius since v_{av} is proportional to R^2 at a constant volumetric flow. The laminar velocity profile will also be significantly steeper close to the sample surface and hence convective transport of oxygen will increase. Modelled velocity profiles between the sample surface and reactor wall are shown for different reactor radii in Fig. 10. The increased longitudinal convective mass transport will also increase the gradient of the concentration boundary layer and increase the driving force for radial diffusion in the gas to further increase the transport of oxygen near the sample surface.

Table 4. Gas stream cross sectional area, A_{CS}, average gas velocity, v_{av}, and Reynolds number, Re, between the sample surface and reactor wall at different reactor radii, R. Sample radius $r = 1$ mm

R [cm]	A_{CS} [cm^2]	v$_{av}$ [m s^{-1}]	Re
1	3.1	0.11	22
0.5	0.75	0.44	38
0.25	0.16	2.0	59

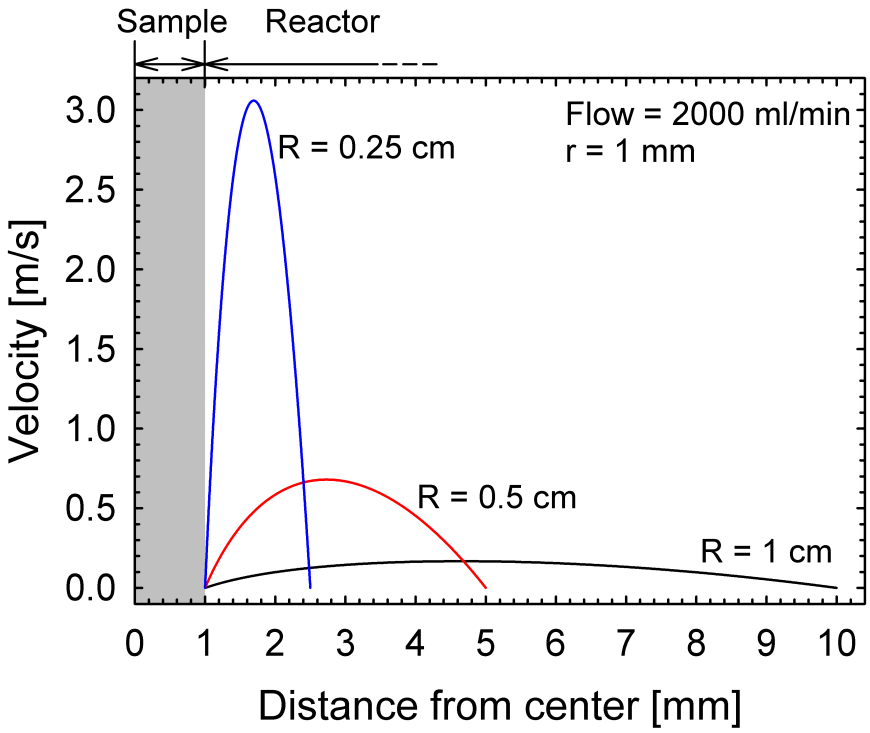

Fig. 10. Modelled laminar velocity profiles between the sample surface and reactor wall for different reactor radii.

The transport coefficients obtained from model runs with different reactor radii are shown in Fig. 11 (a). The deviation in k_{chem} is less for a smaller reactor radius, but even with a radius as small as 0.25 cm, which corresponds to a gap between the sample surface and reactor wall of only 1.5 mm, the accuracy is improved only marginally.

To further increase the transport of oxygen in the gas phase, changing the carrier gas to a gas with lower atomic mass, such as helium, will increase the binary diffusion coefficient of the gas mixture and thus increase the diffusive flux, according to Eq. (9). The difference between using nitrogen and helium as a carrier gas is shown in Fig. 11 (b) and the improvement is evident, however small. The binary diffusion coefficient in an O_2/N_2 gas mixture at 900 °C is $D_{O_2N_2} = 2.1$ cm^2 s^{-1} while for an O_2/He gas mixture $D_{O_2He} = 4.5$ cm^2 s^{-1}. Although the diffusion coefficient increase with a factor >2 the improvement in the apparent transport coefficients is again marginal. It is important to note that using a gas mixture of oxygen and helium in ECR measurements might cause some challenges with respect to temperature. As the heat capacity of a monoatomic gas (e.g. helium) is very different from that of a diatomic gas (e.g. oxygen) [21], a step change in oxygen content will change the heat capacity of the gas. If the gas is not sufficiently heated before entering the reactor, the sample will be cooled by the gas and a change in heat capacity might lead to temperature variations when performing a step change in gas composition.

With the results presented in this section it becomes apparent how sensitive k_{chem} is

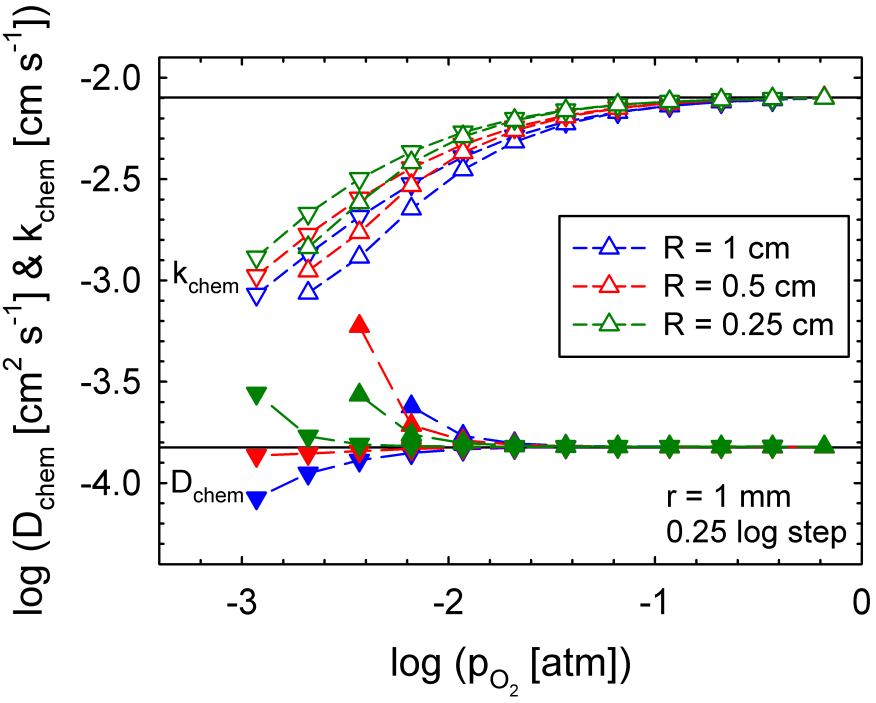

(a)

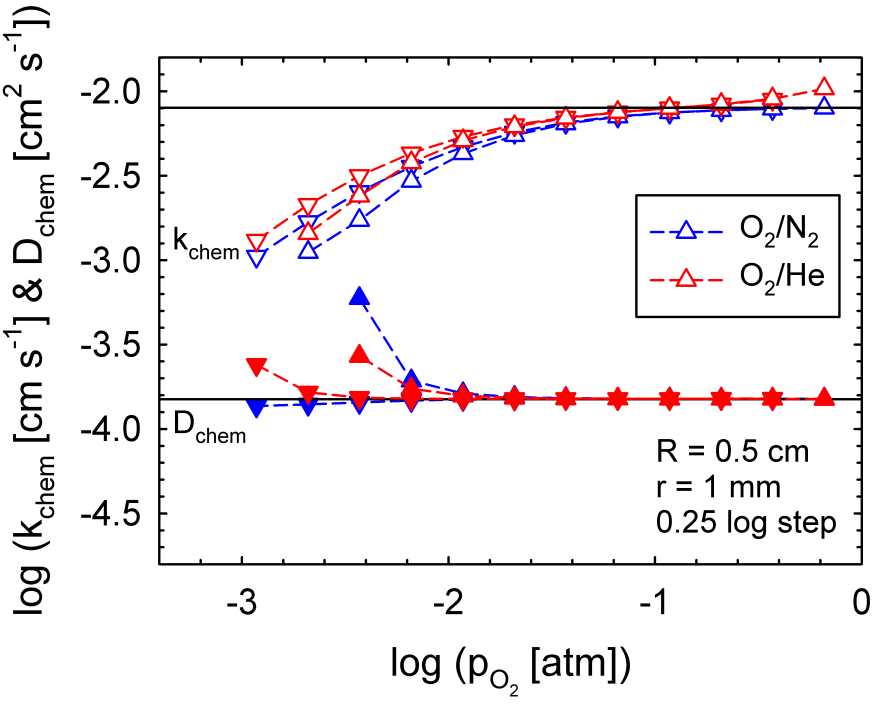

(b)

Fig. 11. Fitted k_{chem} (open symbols) and D_{chem} (closed symbols) from modelled conductivity data with (a) different reactor radii and (b) with different carrier gas. Oxidation values are given as upward triangle symbols while reduction values appear as downward triangle symbols.

on insufficient transport of oxygen in the gas phase and how difficult it is to prevent this and obtain reliable values specifically at low oxygen partial pressures.

4.3 Effect of material properties on gas-phase oxygen diffusion limitations

The degree of influence of mass transport limitations depends on the magnitude of k_{chem} and D_{chem} as well as the total oxygen exchanged, $\Delta\delta$. Thus, the validity of the computed transport coefficient is also dependent on the material in question. Fig. 12 shows the results of modelling with different values of k_{chem} and D_{chem}, respectively. Here one coefficient is changed while the other coefficient is set to a very high value to ensure that the oxygen transport is solely controlled by either surface exchange, Fig. 12 (a), or bulk diffusion, Fig. 12 (b). It is evident that the deviations become less as the transport coefficients are reduced. A slow material will yield a low flux of oxygen across the sample surface and thus not affect the oxygen partial pressure at the sample surface to the same extent as a fast material. Or, in other words, the transport of oxygen in the gas phase is sufficiently fast to maintain the intended oxygen partial pressure close to the surface when the flux of oxygen across the surface is low. This becomes even more clear in Fig. 12 (b), showing that the validity of D_{chem} is shifted significantly to lower p_{O_2} as the magnitude of D_{chem} decrease.

4.4 Temperature dependencies

All the modelled results to this point have been performed at 900 °C and with focus on the p_{O_2} dependencies. Surface exchange and bulk diffusion coefficients are often reported as a function of temperature with calculated activation energies and it is therefore of interest to see how mass transport limitations are affecting the temperature dependencies. In section 4.2 a criteria for the validity of D_{chem} was introduced and by only reporting values that fulfil this measure, obviously the temperature dependence will not be affected by mass transport limitations. Such a simple criteria for the validity of k_{chem} could not be obtained, making it difficult to evaluate the reliability of these coefficients. Thus, the surface exchange coefficient is of particular interest and only k_{chem} will be addressed in this section.

Reported activation energies for k_{chem} are typically in the range 100–200 kJ mol^{-1} and an activation energy $E_{a,k_{chem}} = 100$ kJ mol^{-1} was used for modelling the surface exchange coefficient in this section. The chemical bulk diffusion coefficient was set to a large value ($D_{chem} = 1$ cm^2 s^{-1} $>>$ k_{chem}), thus ensuring surface exchange controlled kinetics. All other material properties are the same as those presented in Table 2. The resulting inverse temperature dependency of $\log k_{chem}$ at different oxygen partial pressures is shown in Fig. 13. It is evident that fitted values of k_{chem} become more reliable at lower temperatures since the surface exchange coefficient becomes smaller and hence the flux across the sample surface decreases. The flow is 500 Nml/min for all model runs, but due to gas expansion the flow through the reactor will be 1800 mL min^{-1} at 850 °C and 1464 mL min^{-1} at 600 °C. The

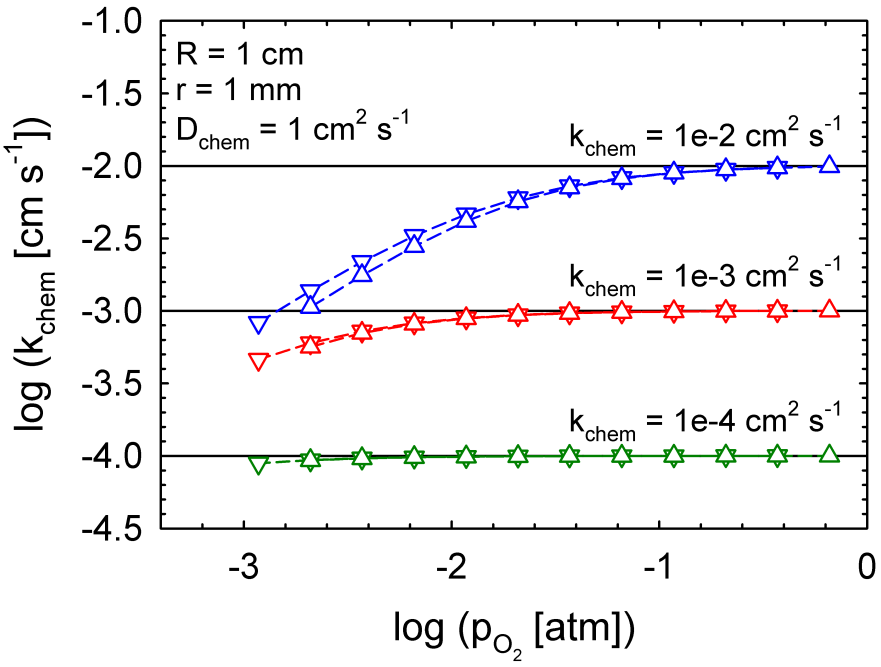

(a)

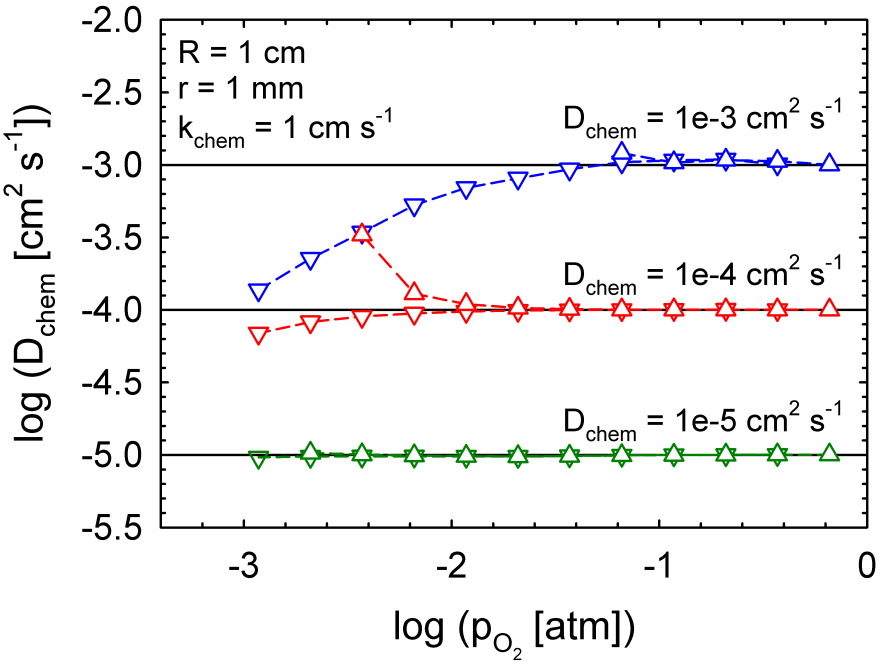

(b)

Fig. 12. (a) Fitted k_{chem} from modelled conductivity data with different set values of k_{chem}. D_{chem} is held constant to a value of 1 $cm^2\,s^{-1}$. (b) Fitted D_{chem} from modelled conductivity data with different set values of D_{chem}. k_{chem} is held constant to a value of 1 $cm\,s^{-1}$. Oxidation values are given in upward triangle symbols while reduction values are given in downward triangle symbols. Solid lines are the true coefficients, broken lines are guide to the eye.

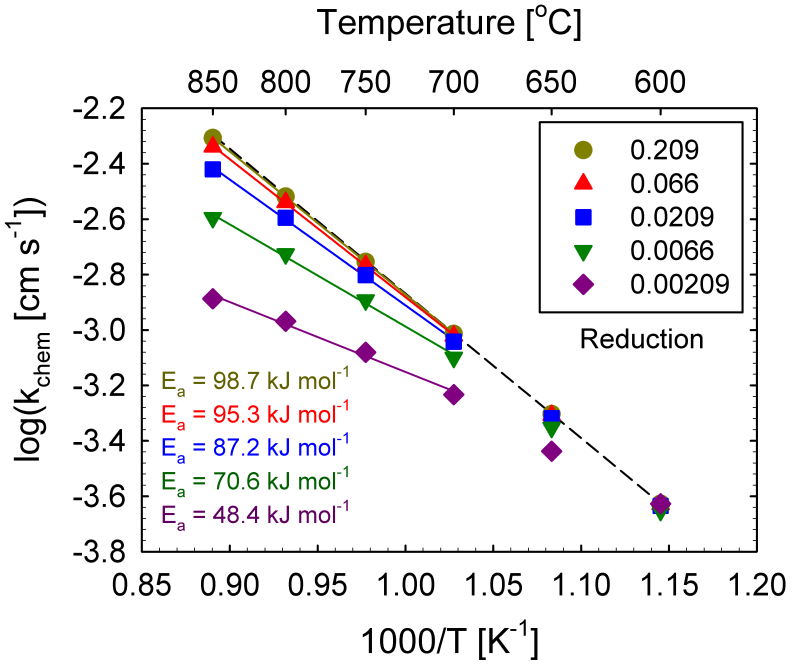

(a)

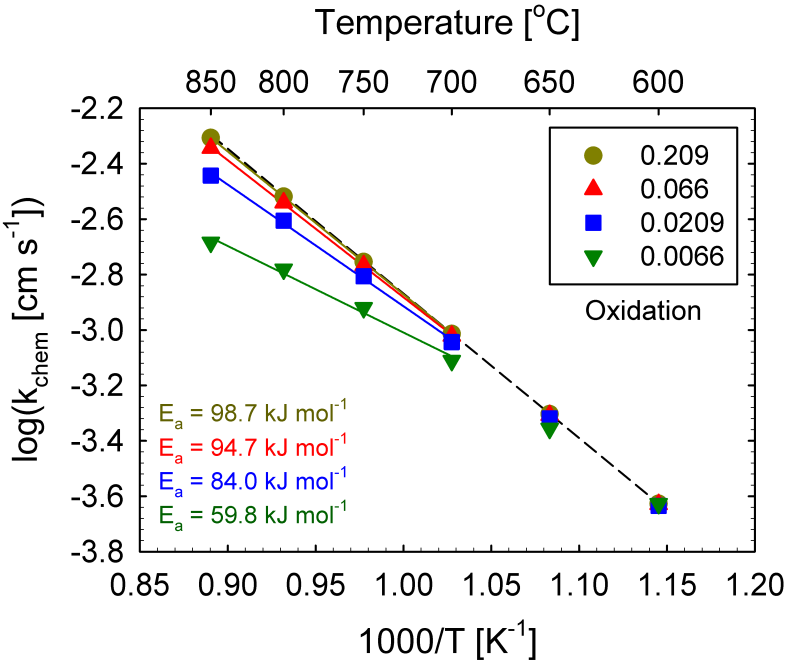

(b)

Fig. 13. Calculated apparent log k_{chem} from modelled conductivity data as a function of inverse temperature. (a) Reduction steps and (b) oxidation steps. Legends give the final p_{O_2} in units of atm. Solid lines are linear fit to the data and the associated activation energies are given. Broken lines are the true coefficients. Modelling performed with half an order of magnitude step size in p_{O_2}, $R = 1$ cm, $r = 1$ mm and $D_{chem} = 1$ cm^2 s^{-1}.

binary diffusion coefficient will also decrease with decreasing temperature, hence mass transport by both diffusion and convection in the gas-phase will be reduced at lower temperatures. However, the change in convection (moderate change in flow) and gas diffusion (small activation energy) are minor compared to that of k_{chem} and hence the computed k_{chem} values at lower temperatures are more reliable. The apparent activation energies are calculated for $T \geq 700$ °C and show a decrease of more than 50% for $p_{O_2} = 2.09 \cdot 10^{-3}$ relative to the true value.

It is clear that in order to increase the reliability of k_{chem} it is favourable to perform ECR measurements at lower temperatures where the effect of mass transport limitation is smaller. By the same reason, data obtained at high temperatures should be critically evaluated to avoid reporting erroneous activation energies.

4.5 General recommendations concerning the assessment of k_{chem} and D_{chem}

A criteria for the absolute lowest oxygen partial pressure at which reliable bulk diffusion coefficients may be obtained for a given experiment can be assessed where the computed apparent D_{chem} show a splitting between oxidation and reduction values. However, the deviation in k_{chem} may be significant also at these oxygen partial pressures and the obtained values of k_{chem} should be critically evaluated. For a given experimental setup, measurements at high p_{O_2} and low temperatures is favourable to decrease the extent of mass transport limitations. As a general advice (rule of thumb) for materials exhibiting high oxygen exchange rates, measurements at $\log p_{O_2} \gtrsim -1$ should be avoided for temperatures $T \gtrsim 800$ °C as mass transport limitations are likely to be pronounced in this region.

The step size have been shown to have only minute effect on the deviation of k_{chem} due to mass transport limitations. A small step size reduces the apparent splitting between oxidation and reduction values of k_{chem}, but do not improve the validity of the surface exchange coefficients at low p_{O_2}. The experimental setup has been shown to have an effect on the mass transport limitations. However, the resulting improvements in the computed surface exchange and bulk diffusion limitations are somewhat limited. In general, the radius of the reactor, or the cross sectional area for gas flow along the sample, should be as small as possible and the volumetric flow rate should be chosen as high as possible. Both of which will increase the convective mass transport in the gas phase, as well as the diffusive gas transport across the boundary layer. However, an increase in volumetric flow rate may also involve the necessity of preheating of the gas to avoid effects of sample cooling. The diffusive mass transport in the gas phase may also be improved by choosing a carrier gas with a low atomic mass, e.g. helium, however, the effect on the accuracy of k_{chem} and D_{chem} is shown to be marginal.

5 Conclusions

The effect of mass transport limitations in the gas phase on the assessment of k_{chem} and D_{chem} from ECR measurements has been investigated using a finite element model. A pronounced effect of mass transport in the gas phase was shown, especially for materials exhibiting high oxygen exchange rates and/or at low oxygen partial pressures. A pronounced splitting of oxidation and reduction values for both k_{chem} and D_{chem} was shown when mass transport limitations were pronounced. Modelled apparent activation energies of k_{chem} were shown to decrease significantly with increasing mass transport limitations. A criteria for the validity of D_{chem} was introduced stating that computed bulk diffusion coefficients can be trusted when no significant discrepancy between oxidation and reduction values is evident. No such measure could be obtained for k_{chem}, making it difficult to evaluate the reliability of calculated surface exchange coefficients from ECR measurements. However, as a general advice for materials exhibiting large oxygen exchange rates, measurements at $p_{O_2} < 1 \cdot 10^{-1}$ atm should be avoided for temperatures $T \gtrsim 800$ °C. Decreasing the p_{O_2} step size showed no effect on the mass transport limitations while changing the experimental parameters to increase convective and diffusive transport in the gas phase (e.g. increase the velocity or change the carrier gas to a gas of low atomic mass) yielded an improvement of the results. The improvements were, however, marginal and the surface exchange coefficient showed extremely sensitive to insufficient transport of oxygen in the gas phase.

Electrical conductivity relaxation as a method for assessing the chemical surface exchange and bulk diffusion coefficients was shown to be sensitive to mass transport limitations. However, true values can be obtained by performing measurements at high oxygen partial pressures and/or at low temperatures. Calculated surface exchange coefficients at high temperatures or low partial pressures should be treated carefully as the reliability of the coefficients with respect to the effect of mass transport limitations is difficult to evaluate.

Nomenclature

Bold characters denote vector quantities

A	[m^2]	Area
C	[mol m^{-3}]	Concentration
D_{chem}	[cm^2 s^{-1}]	Chemical bulk diffusion coefficient
D_{ij}	[cm^2 s^{-1}]	Binary gas diffusion coefficient
$\mathbf{E}$	[V m^{-1}]	Electric field
I	[A]	Electric current
$\mathbf{j}$ (j)	[kg m^{-2} s^{-1}]	Diffusive mass flux
$\mathbf{J}$ (J)	[mol m^{-2} s^{-1}]	Diffusive molar flux
$\mathbf{J}_c$	[A m^{-2}]	Current density
k_{chem}	[cm s^{-1}]	Chemical surface exchange coefficient
M	[g mol^{-1}]	Molar volume
$\mathbf{n}$ (n)	[kg m^{-2} s^{-1}]	Total mass flux
$\mathbf{N}$ (N)	[mol m^{-2} s^{-1}]	Total molar flux
p	[Pa]	Total pressure
p_{O_2}	[atm]	Partial pressure of oxygen
r	[mm]	Sample radius
R	[cm]	Reactor radius
T	[°C]	Temperature
$\mathbf{v}$ (v)	[m s^{-1}]	Velocity
x		Mole fraction
δ		Oxygen non-stoichiometry
ρ	[kg m^{-3}]	Density
ω		Mass fraction
σ	[S cm^{-1}]	Electric conductivity

Subscripts

av	Average
bulk	Bulk
cs	Cross section
eq	Equilibrium
i	The ith species
j	The jth species
O_2	Molecular oxygen
O	Monoatomic oxygen
src	Source
surf	Surface
term	Terminal

Acknowledgment

Funding provided by the Norwegian Research Council (NFR), FRINAT-project no. 191358: The kinetics of surface exchange reactions in oxide based mixed conductors at reducing conditions and high temperatures, is acknowledged.

A Calculation of chemical surface exchange and bulk diffusion coefficients

A change in the oxygen partial pressure will in practical cases not be a discrete step but rather a continuous change over time depending primarily on the flow rate and reactor cross section. The change in oxygen partial pressure may be described by an exponential function, viz.:

$$\frac{p_{O_2}(t) - p_{O_2,t=\infty}}{p_{O_2,t=0} - p_{O_2,t=\infty}} = \exp\left(-\frac{t}{\tau_f}\right) \tag{18}$$

where τ_f is the reactor flush time constant. The solution of Eq. (2) for a long cylindrical sample (1-dimensional) using the change in oxygen partial pressure as described in Eq. (18) have been described by den Otter et al. [8] and are given below in terms of sample mass, M:

$$\begin{aligned}\frac{M(t) - M_0}{M_\infty - M_0} =& 1 - \exp\left(-\frac{t}{\tau_f}\right) \\ &- \sum_{n=1}^{\infty} A_n \cdot \frac{\tau_n}{\tau_n - \tau_f} \cdot \left[\exp\left(-\frac{t}{\tau_n}\right) - \exp\left(-\frac{t}{\tau_f}\right)\right]\end{aligned} \tag{19}$$

where $M(t)$ is the sample mass, respectively, at any given time ($t = t$) and subscripts 0 and ∞ denotes the mass at time $t = 0$ and $t = \infty$, respectively. The parameter A_n is given by

$$A_n = \frac{2L_\rho^2}{\rho_n^2(\rho_n^2 + L_\rho^2 + L_\rho)} \tag{20}$$

and

$$\tau_n = \frac{r^2}{\rho_n^2 D_{chem}} \tag{21}$$

where r is the sample radius. The parameter L_ρ and the eigenvalue ρ_n are solved from

$$\rho_n J_1(\rho_n) = L_\rho J_0(\rho_n) = \frac{r k_{chem}}{D_{chem}} J_0(\rho_n) \tag{22}$$

where J_0 and J_1 denotes the first and second Bessel functions of the first kind.

As a criterion for applying conductivity relaxation to assess the transport coefficients of a material, the conductivity, σ, must be linearly proportional to the oxygen non-stoichiometry, $3 - \delta$. When this criterion is fulfilled, the relation between the

conductivity and total mass change of the sample, due to a change in oxygen non-stoichiometry, is given by [14]:

$$\frac{\sigma(t) - \sigma_0}{\sigma_\infty - \sigma_0} = \frac{M(t) - M_0}{M_\infty - M_0} \tag{23}$$

where σ is the total conductivity. Eq. (23) can be substituted in on the left side of Eq. (19) and the conductivity response on a change in partial pressure in oxygen can thus be used to calculate D_{chem} and k_{chem}.

References

[1] H. J. M. Bouwmeester, Dense ceramic membranes for methane conversion, Catalysis Today 82 (1-4) (2003) 141–150.

[2] M. Søgaard, P. Vang Hendriksen, M. Mogensen, Oxygen nonstoichiometry and transport properties of strontium substituted lanthanum ferrite, Journal of Solid State Chemistry 180 (4) (2007) 1489–1503.

[3] J. E. ten Elshof, M. H. R. Lankhorst, H. J. M. Bouwmeester, Oxygen exchange and diffusion coefficients of strontium-doped lanthanum ferrites by electrical conductivity relaxation, Journal of the Electrochemical Society 144 (3) (1997) 1060–1067.

[4] I. Wærnhus, T. Grande, K. Wiik, Surface exchange of oxygen in $La_{1-x}Sr_xFeO_{3-\delta}$ (x = 0, 0.1), Topics in Catalysis 54 (13-15) (2011) 1009–1015.

[5] E. Bucher, A. Egger, P. Ried, W. Sitte, P. Holtappels, Oxygen nonstoichiometry and exchange kinetics of $Ba_{0.5}Sr_{0.5}Co_{0.8}Fe_{0.2}O_{3-\delta}$, Solid State Ionics 179 (21-26) (2008) 1032–1035.

[6] W. Preis, E. Bucher, W. Sitte, Oxygen exchange kinetics of $La_{0.4}Sr_{0.6}FeO_{3-\delta}$ by simultaneous application of conductivity relaxation and carrier gas coulometry, Solid State Ionics 175 (1-4) (2004) 393–397.

[7] H. J. M. Bouwmeester, M. W. Den Otter, B. A. Boukamp, Oxygen transport in $La_{0.6}Sr_{0.4}Co_{1-y}Fe_yO_{3-\delta}$, Journal of Solid State Electrochemistry 8 (9) (2004) 599–605.

[8] M. W. Den Otter, H. J. M. Bouwmeester, B. A. Boukamp, H. Verweij, Reactor Flush Time Correction in Relaxation Experiments, Journal of the Electrochemical Society 148 (2) (2001) J1–J6.

[9] R. Ben Mansour, M. A. Nemitallah, M. A. Habib, Numerical investigation of oxygen permeation and methane oxy-combustion in a stagnation flow ion transport membrane reactor, Energy 54 (2013) 322–332.

[10] J. M. Gozálvez-Zafrilla, A. Santafé-Moros, S. Escolástico, J. M. Serra, Fluid dynamic modeling of oxygen permeation through mixed ionic-electronic conducting membranes, Journal of Membrane Science 378 (1-2) (2011) 290–300.

[11] S. B. Adler, J. A. Lane, B. C. H. Steele, Electrode kinetics of porous mixed-conducting oxygen electrodes, Journal of the Electrochemical Society 143 (11) (1996) 3554–3564.

[12] B. E. Poling, J. P. O'Connell, J. M. Prausnitz, The properties of gases and liquids, McGraw-Hill, New York, 2001.

[13] F. A. Kröger, H. J. Vink, Relations between the Concentrations of Imperfections in Crystalline Solids, Solid State Physics 3 (C) (1956) 307–435.

[14] I. Yasuda, T. Hikita, Precise determination of the chemical diffusion coefficient of calcium-doped lanthanum chromites by means of electrical conductivity relaxation, Journal of the Electrochemical Society 141 (5) (1994) 1268–1273.

[15] J. Crank, The mathematics of diffusion, Clarendon Press, Oxford, 1975.

[16] R. B. Bird, W. E. Stewart, E. N. Lightfoot, Transport phenomena, 2nd Edition, Wiley, New York, 2007.

[17] D. N. Mueller, R. A. De Souza, H. I. Yoo, M. Martin, Phase stability and oxygen nonstoichiometry of highly oxygen-deficient perovskite-type oxides: A case study of (Ba,Sr)(Co,Fe)$O_{3\delta}$, Chemistry of Materials 24 (2) (2012) 269–274.

[18] Ø. F. Lohne, Oxygen non-stoichiometry and electrical conductivity of $La_{0.2}Sr_{0.8}Fe_{0.8}B_{0.2}O_{3-\delta}$ where B = Fe, Al, Ti, Ta, Paper 1 in this thesis.

[19] M. H. R. Lankhorst, H. J. M. Bouwmeester, H. Verweij, High-Temperature Coulometric Titration of $La_{1-x}Sr_xCoO_{3-\delta}$: Evidence for the Effect of Electronic Band Structure on Nonstoichiometry Behavior, Journal of Solid State Chemistry 133 (2) (1997) 555–567.

[20] M. H. R. Lankhorst, J. E. Ten Elshof, Thermodynamic Quantities and Defect Structure of $La_{0.6}Sr_{0.4}Co_{1-y}Fe_yO_{3-\delta}$ (y=0–0.6) from High-Temperature Coulometric Titration Experiments, Journal of Solid State Chemistry 130 (2) (1997) 302–310.

[21] S. Stølen, T. Grande, N. L. Allan, Chemical thermodynamics of materials: macroscopic and microscopic aspects, Wiley, Chichester, 2004.